Aalborg Universitet

State of health estimation of second-life lithium-ion batteries under real profile operation

Elisa Braco[1,2], Idoia San Martín[1], Pablo Sanchis[1], Alfredo Ursúa[1,*], Daniel-Ioan Stroe[2]

(1) Institute of Smart Cities (ISC), Department of Electrical, Electronic and Communications Engineering, Public University of Navarre (UPNA), Campus de Arrosadia, 31006 Pamplona, Spain

(2) Energy Department, Aalborg University, Pontoppidanstraede 101, 9220 Aalborg, Denmark

Abstract

The economic viability of second-life (SL) Li-ion batteries from electric vehicles (EVs) is still uncertain nowadays. Assessing the internal state of reused cells is key not only at the repurposing stage but also during their SL operation. As an alternative of the traditional capacity tests used to this end, the estimation of State of Health (SOH) allows to reduce the testing time and the need of equipment, thereby reinforcing the economic success of SL batteries. However, the estimation of SOH in real SL operation has been rarely analysed in literature. This contribution aims thus to cover this gap, by focusing on the experimental assessment of SOH estimation in reused modules from Nissan Leaf EVs under two SL scenarios: a residential household with self-consumption and a fast charge station for EVs. By means of partial charge and experimental data from cycling and calendar ageing tests, accuracy and robustness of health indicators is firstly assessed. Then, SOH estimation is carried out using real profiles, covering a SOH range from 91.3 to 31 %. Offline assessment led to RMSE values of 0.6 % in the residential profile and 0.8 % in the fast charge station, with a reduction in testing times of 85 % compared to a full capacity test. In order to avoid the interruption of battery operation, online assessment in profiles was also analysed, obtaining RMSE values below 1.3 % and 3.6 % in the in the residential and charging station scenarios, respectively. Therefore, the feasibility of SOH estimation in SL profiles is highlighted, as it allows to get accurate results reducing testing times or even without interrupting normal operation.

Keywords: Lithium-ion battery, Second-life batteries, State of health estimation, Residential storage, Fast charge station

*Corresponding author. Email address: alfredo.ursua@unavarra.es

Nomenclature

C Capacity

C_N Nominal capacity

CC Constant current

CV Constant voltage

DOD Depth of discharge

EIS Electrochemical impedance spectroscopy

EV Electric vehicle

F_I Current adjustment factor for extracting conditions of PCM

F_T Temperature adjustment factor for extracting conditions of PCM

F_V Voltage adjustment factor for extracting conditions of PCM

FL First life

HI Health indicator

IC Incremental capacity

ICA Incremental capacity analysis

LR Linear regression

$MaxAE$ Maximum absolute error

$mid-SOC$ Middle state of charge in a cycle

PC Partial charge

PCC Pearson correlation coefficient

PCM Partial charging method

$RMSE$ Root mean squared error

RPT Reference performance test

SL Second life

SOC State of charge

SOH State of health

$SVR–L$ Support vector regression with linear kernel

$SVR–RBF$ Support vector regression with radial basis function kernel

V_S Charging starting voltage

1. Introduction

Electric vehicle (EV) has become a major actor in the automotive sector nowadays. The environmental problems related to traditional combustion vehicles, together with government regulations and citizen awareness have contributed to the expansion of EVs, a trend that is expected to continue in the future. As a result, the demand for Li-ion EV batteries is growing year by year, reaching 160 GWh only in 2020 [1].

The performance of Li-ion batteries are negatively affected by usage, in such a way that their capacity and power fade. This eventually compromises EV requirements, and as a result, automotive standards set a capacity fade of 20 to 30 % from the nominal value as withdrawal limit. Once retired from EVs, the reuse of these batteries emerges as an alternative to direct recycling. The resulting enlargement of lifetime represents an interesting solution both from an environmental and economic perspective [2, 3]. Stationary applications, such as residential storage, electric microgrids or grid integration of renewable energies, in which energy and power requirements are less demanding than in EVs are promising scenarios for the second life (SL) of these EV batteries [4, 5, 6, 7, 8].

However, the success of SL batteries from EVs is not yet clear nowadays, as there are some uncertainties related to the technical and economic viability of these systems [2, 3]. Operation and durability of SL modules [9, 10, 11], and battery packs [12, 13] has experimentally been assessed, but there are still doubts concerning economic feasibility.

In this context, a key aspect in SL is the assessment of the battery state. Capacity and internal resistance of reused modules may vary from the automotive withdrawal limits when retired from EVs as a consequence of their first usage [9, 14, 15]. Hence, it is necessary to ensure the compliance with requirements in SL applications. Moreover, battery repurposing with similar modules allows to reduce performance dispersion, which contributes to extend battery life and consequently profitability. The need of characterisation is therefore clear at the repurposing stage, but attention should also be paid during SL operation. At advanced stages of ageing, the degradation rates of Li-ion cells accelerate, as a consequence of a shift in the main ageing mechanisms [11]. This involves higher risks in operation, as chances of internal short circuits increase [16]. Therefore, the operation in SL should be restricted before this turning point. Moreover, reused modules may suffer from uneven degradation trends even under similar ageing conditions [11], which also confirms that the knowledge of their performance capabilities is also needed during operation in order to ensure safety.

The state of health (SOH) of batteries can be obtained offline or online. Offline refers to the fact that it is necessary for the battery to stop operating in order to estimate the SOH, while online refers to the estimation of the SOH in real operation. The SOH of Li-ion batteries is traditionally assessed by means

3

of capacity and/or internal impedance tests. This generally requires several hours of testing, as well as specific equipment. Moreover, the normal operation of the batteries has to be interrupted to perform the tests. With regard to reduce SL costs and procedures, SOH estimation is considered as a promising alternative to traditional characterisation tests. This approach is based on the identification of a parameter related to SOH, i.e., a health indicator (HI), from which SOH can be assessed by different methods [17, 18]. Thus, from experimental testing it is possible to extract HIs from direct measurements such as impedance [19], voltage [20, 21, 22] or charging curve [10], or indirect analysis such as incremental capacity analysis (ICA) [10, 23] or partial charging method (PCM) [24, 25, 26]. Then, on a second stage, two main groups of methods arise, depending on HI assessment: machine learning methods and model-based adaptive filters. The first gathers examples such as neural networks [27] or support vector regression (SVR) algorithms [20, 22, 24], which are used to directly evaluate HIs. Despite their accuracy, these methods are difficult to implement online, given that operating conditions may vary from laboratory environment and that the interruption of normal operation could be needed [28, 29]. On the other hand, adaptive methods such as Kalman filters [30] address the internal state variables through iteration and look-up tables with ageing data. The high accuracy of these alternatives is counterbalanced with the complexity of the calculations required, which may compromise their implementation in real systems [17].

Thereby, the estimation of SOH with real profile operation is still a challenge nowadays [17]. Renewable energies integration [29], frequency regulation [20, 22] or EV operation [31] are some of the scenarios covered in previous research works, though SOH values over 80 % are normally assessed. When it comes to SL analysis, most research focuses on the repurposing stage [10, 14, 19, 23, 25], covering SOH over 60 %. However, only few contributions analyse the online operation of retired batteries during SL lifetime. In [24], the authors assessed PCM by means of SVR in retired NMC and LFP cells under a synthetic cycling profile, achieving RMSE below 1.9 % in a SOH range from 80 to 45 %. From its part, [10] evaluated several HIs such as EIS, ICA or Average Fréchet Distance, both in offline and online approaches also using synthetic cycling. In this case, the SOH covered 94 to 62 %, obtaining mean errors of 1.5 %. Table 1 summarises the main contributions identified above, which are classified according to HI method, algorithm, application, online or offline approach and for FL or SL batteries.

As can be seen, only few steps have been taken in SOH estimation using SL batteries under dynamic profiles. Hence, this contribution aims to cover this gap, by considering retired Li-ion cells from EVs, which are further aged under real profiles. The experimental results will add valuable information for the economic end technical viability of SL batteries. The paper is organised as follows. Section 2 describes the experimental procedure, covering modules and testing setup. Section 3 details the SOH estimation method, including feature

Table 1: Research contributions targeting SOH estimation for Li-ion batteries

Ref.	HI Method	Algorithm	Application	Estimation	Battery
[10]	Charging curve/ ICA/ EIS/ AFD	LR	-	Offline/ Online	SL
[19]	Impedance	LR	-	Offline	SL
[20]	Voltage	SVR	Frequency regulation	Online	FL
[21]	Voltage	Multiple linear regression	-	Offline	FL
[22]	Voltage	SVR	Frequency regulation	Offline	FL
[23]	ICA	Least square regression	Frequency regulation	Offline	SL
[24]	PCM	SVR	-	Online	SL
[25]	PCM	Machine learning	Repurposing stage	Offline	SL
[27]	ICA	Neuronal networks	-	Online	SL

extraction and selection, as well as model development. Section 4 describes the SL profiles analysed: a residential household with self-consumption and a fast charging station for electric buses. The experimental results obtained are gathered in Section 5, including HI assessment and selection and the validation of SOH models in offline and online approaches. Finally, Section 6 draws the main conclusions of the work.

2. Experimental setup

2.1. Module description

The experimental procedure of this contribution has been carried out with Li-ion battery modules specially designed for automotive purposes, in particular for Nissan Leaf EVs. Each module is formed by four pouch-type cells of nickel and manganese oxide (LMO-NMO) cathode and graphite anode. These cells are connected in pairs and associated in series (2s2p), i.e. the cells are configured by series connection of two pairs of cells connected in parallel, in such a way that three terminals are available: positive, middle point and negative. Therefore, 2p cells are the smallest testing unit. The nominal capacity (C_N) of the modules is 66 Ah, and their maximum, minimum, and nominal voltages are 8.3 V, 5 V, and 7.5 V, respectively; and the C_N of each pair of cells (2p) is also 66 Ah and their maximum, minimum, and nominal voltages are 4.15 V, 2.5 V, and 3.75 V, respectively. Fig. 1 shows the experimental setup, with the Nissan Leaf modules connected to the battery tester, and inside the climatic chamber.

According to their previous usage, two types of modules have been tested. On the one hand, 12 modules retired from different EVs are analysed, which
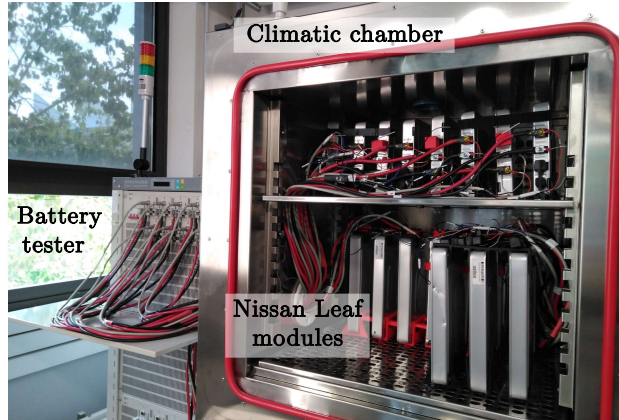
Figure 1: Example of Nissan Leaf modules under test and experimental test bench.

will be referred to as SL modules. The specific usage data of these SL modules is unknown, as the manufacturer does not provide such information nowadays. On the other hand, 5 modules which have never been used in EVs are also analysed. Given their lack of usage, they are named as first-life (FL) modules. In this case, they correspond to spare samples which have been stored for a long time, and therefore may have suffered from degradation due to calendar ageing.

2.2. Experimental procedure

The experimental tests carried out in this work is divided into two groups: reference performance tests (RPT) and ageing tests. All the experimental procedures have been performed at 2p cell level between positive and middle point terminals. This 2p association will be hereinafter named as cell in order to ease reading.

2.2.1. Reference performance test

RPTs aim to assess the SOH of the cells. To this end, they are based on capacity tests, consisting of two full charging-discharging cycles at C/3 within the voltage limits of the cell. The charging procedure is constant current (CC) until the maximum cell voltage ($V_{max} = 4.15$ V) followed by a constant voltage (CV) phase until a cut-off current of C/30 is reached. For its part, the discharge procedure is CC until the minimum cell voltage is reached ($V_{min} = 2.5$ V). The current capacity of the cell capacity is considered as the discharged Ah during the second cycle. The charging and discharging rate is defined according to C_N, thereby corresponding 1C = 66 A. Two types of RPTs are carried out, depending on the testing temperature:

a) **RPT$_{25}$.** To assess the actual state of the cell, RPT$_{25}$ consist of a capacity test carried out at a controlled ambient temperature of 25 °C±1 °C. Prior to each RPT$_{25}$, a rest time of 4 hours is set at the given temperature, so

6

that the cell reaches thermo-dynamic equilibrium. Then, capacity test starts with a CC discharge pulse at C/3 until the minimum voltage of the cell. The capacity value obtained from this test is considered as the actual state of the cell (C).

b) **RPT$_{45}$.** During the cycling ageing test, periodical capacity tests are performed at 45 °C±1 °C to evaluate the state of the cell. Prior to them, the cell is discharged with a CC pulse at C/3 until the minimum voltage. After the capacity test, the cell is CCCV charged and CC discharged at C/2 between its voltage limits and with C/30 as cut-off current of the CV phase.

2.2.2. Ageing tests

The robustness of the HIs to ageing is analysed by means of a set of accelerated ageing tests. Both cycling and calendar tests are carried out, so that different ageing conditions are covered. Moreover, a set of cells are aged under two real profiles of SL applications.

a) **Cycling.** Cycling ageing is mainly influenced by temperature, cycle depth of discharge (DOD), middle state of charge (mid-SOC) and C-rate. These parameters do not have a linear influence on degradation, and therefore several conditions should be tested to get representative results. The cycling ageing matrix of this contribution targets DOD and mid-SOC, and contains 10 different conditions, with a total of 6 DOD levels performed at different mid-SOC. All the cycling ageing tests are carried out under a controlled ambient temperature of 45 °C±1 °C. The test starts with a 4-hour rest and a CC discharge at C/3 until the minimum cell voltage, followed by an RPT$_{45}$. The cell is then charged at C/3 until the corresponding mid-SOC. After a 1-hour rest, the cycling sequence with CCCV charges and CC discharges at 0.7C is applied with the corresponding DOD. The cut-off current is C/30 in all cases. Both mid-SOC and DOD are computed from the corresponding actual capacity. Every 100 equivalent full cycles (EFC), a 1 hour rest is set, followed by a RPT$_{45}$. EFC is defined as the ratio between the Ah throughput of the cell and twice C_N. Every 4 weeks a RPT$_{25}$ is performed. The complete cycling test matrix is summarized in Table 2. As can be seen, a SL cell is tested under each condition, except from 50–60 % SOC, where a FL cell is used. Both in 50–100 % and 0–100 % a SL and a FL cell are aged.

b) **Calendar.** A SL cell is tested under calendar ageing, being stored fully charged at a controlled temperature of 45 °C±1 °C. The test is interrupted every 4 weeks to perform a RPT$_{25}$, so that its actual SOH is assessed. After the RPT$_{25}$, the cell is fully charged at C/3 with CCCV procedure and C/30 as cut-off current.

c) **SL real profiles.** The real profile tests are carried out at a controlled ambient temperature of 45 °C±1 °C. A 4-hour rest is set prior to the test to ensure thermal stability in the cells. Every 2 weeks, a RPT$_{25}$ is performed. The details about the operating conditions of the profiles are given in Section 4.

Table 2: Cycling ageing test matrix.

Cycle depth (%)		5	10	25	50	80	100
SOC range (%)	SL	22.5–27.5	70-80	50–75	50–100	10–90	0–100
		50–55	90-100				
		95–100					
	FL		50-60		50-100		0-100

A FL and a SL sample are tested under each profile. The scaling from real scenario is carried out in terms of energy, considering the original storage system and the energy of the cell at the beginning of the test, obtained from RPT_{25}.

2.2.3. Test bench

The test bench used consists of two battery testers and climatic chamber, as shown in Fig. 1. The multichannel battery testers stand 5 V and 50 A on each channel, with an accuracy within ± 0.1 % of their full scale. The climatic chambers allow a temperature range from -30 °C to +180 °C, with a measurement precision of ± 0.5 °C.

3. SOH estimation method

SOH is a reference of the degradation state of Li-ion batteries, and it can be related to their capacity, energy or power capability. In this contribution, SOH will be defined as the ratio between the actual capacity, measured in RPT_{25}, and the nominal value, according to Eq. (1):

$$SOH(\%) = \frac{C}{C_N} \cdot 100 \tag{1}$$

Thus, from battery operating data of temperature, voltage or current, HIs are first identified, and in a second step they are related to SOH by means of a model. The selection of HI depends on the estimation approach in real profiles, as several criteria such as accuracy or extraction time can be desired. The SOH estimation method followed in this contribution is presented in Fig. 2. As can be seen, the procedure starts with the analysis of ageing tests. Once HI are extracted, a complete analysis is carried out, covering three main aspects. First, a set of factors to adjust the extraction conditions are obtained. Secondly, HIs are assessed in terms of accuracy and extraction time, so that selection criteria for them are defined. Finally, a SOH estimation model is developed. This information is used in the estimation with real profiles, in such a way that after selecting the approach (offline or online), HIs are extracted and selected with the corresponding criteria. If necessary, the extraction conditions will be adapted so

that they match the model. The estimation is finally carried out with the model previously developed. The intermediate steps of the SOH estimation method are further described in this section.
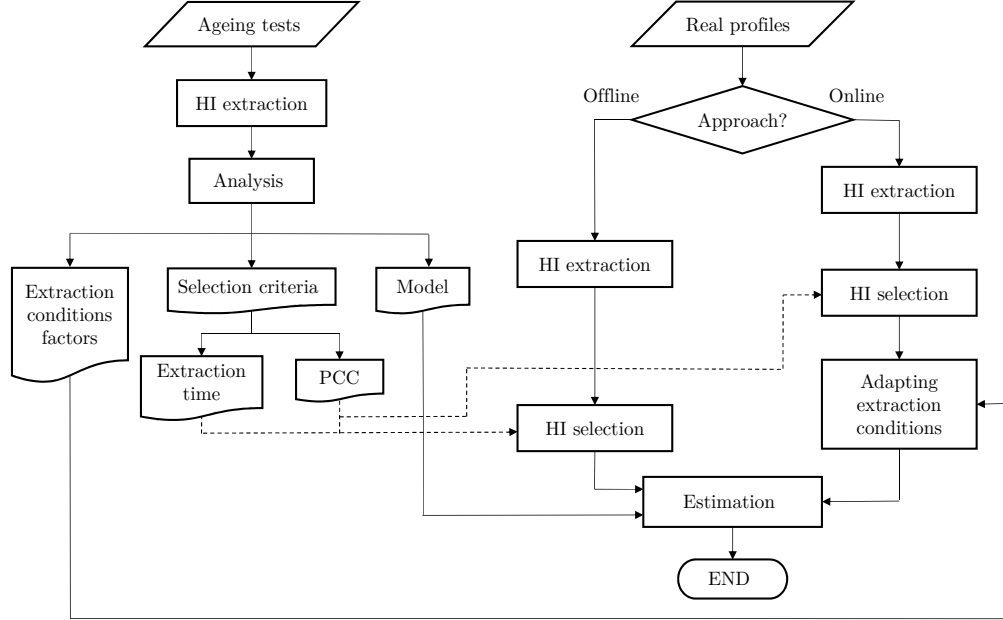
Figure 2: Flowchart of the SOH estimation method for real profiles.

3.1. Feature extraction

3.1.1. Partial charging method

There are several HI extraction methods proposed in literature, such as ICA, PCM, internal resistance and amount of charge of the CC and CV phase. The choice between them is generally based on measurement easiness and accuracy. Considering its promising results in SL batteries, PCM is selected as extraction procedure [32]. This approach is based on the concept that the overall capacity of a cell can be estimated from a given partial charge measured within a specific voltage range [26]. The interest of PCM lays thereby on two reasons. First, HIs can be easily extracted from battery operation, as only coulomb counting is required. Secondly, PCM can be easily implemented in real operation, as charging currents are usually constant, while discharging currents are determined by the load.

The HI extracted from PCM are defined within a voltage range from 3.7 V to 4.15 V, and with voltage intervals of 5 mV. Lower voltage values are not considered, given that there is barely any capacity variation with voltage for the specific chemistry under study [33]. Thereby, 45 HIs are obtained. Table 3

gathers them, specifying their corresponding lower (V_{low}) and upper (V_{high}) voltage.

Table 3: Health indicators (HIs) extracted from PCM with their lower (V_{low}) and upper voltage (V_{high}).

V_{high} (V)	V_{low} (V)								
	3.70	3.75	3.80	3.85	3.90	3.95	4.00	4.05	4.10
3.75	HI 1								
3.80	HI 2	HI 10							
3.85	HI 3	HI 11	HI 18						
3.90	HI 4	HI 12	HI 19	HI 25					
3.95	HI 5	HI 13	HI 20	HI 26	HI 31				
4.00	HI 6	HI 14	HI 21	HI 27	HI 32	HI 36			
4.05	HI 7	HI 15	HI 22	HI 28	HI 33	HI 37	HI 40		
4.10	HI 8	HI 16	HI 23	HI 29	HI 34	HI 38	HI 41	HI 43	
4.15	HI 9	HI 17	HI 24	HI 30	HI 35	HI 39	HI 42	HI 44	HI 45

3.1.2. HI extraction conditions

The specific charge that can be stored in a Li-ion cell depends on measurement conditions such as temperature, C-rate and charging starting voltage (V_S), as well as on the degradation level of the cell, i.e. its SOH [34]. This represents a challenge for PCM, as the comparison between measurements under different extraction conditions could compromise the accuracy of SOH estimation. Hence, the adjustment of these variables is necessary if charges extracted under different conditions are to be compared.

Fig. 3 shows an example of this issue, with cell charge under different conditions of C-rate, V_S, temperature, and SOH. The SOH of the cells in the figure is 65 %, otherwise specified. As an illustrative example, HI 37 is selected, i.e. the charge measured between V_{low}= 3.95 V and V_{high}= 4.05 V. A total of 6.6 Ah were obtained within this voltage range at C/3 and 25 °C with a full charge ($V_S = V_{min}$). When increasing temperature to 45 °C at the same C-rate and maintaining full charge, the extracted charge is 8.9 Ah, thereby 35.1 % greater than at 25 °C. On the other hand, the influence of C-rate can be compared at 45 °C. The measured charges of this HI are 7.6 Ah and 6.8 Ah at C/2 and 0.7C respectively, resulting in values 14.7 % and 23.2 % lower than at C/3 at this temperature. The effect of V_S is also clear, as the HI measured is 3.9 Ah when starting at the example shown ($V_S = 3.91$ V), thus 64.0 % lower than with full charge at the same temperature and current. The effect of ageing can also be seen in this figure, as HI 37 decreases 51.7 % between 65 % and 36 % of SOH, i.e. from 8.9 Ah to 4.3 Ah.
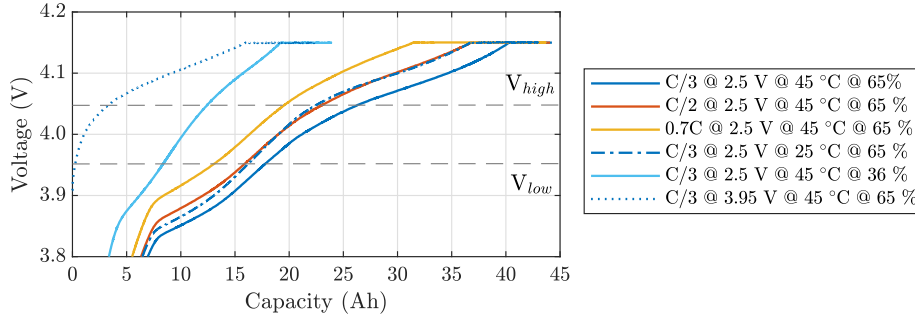
Figure 3: Example of PCM with different extraction conditions detailed for HI37 (3.95 V - 4.05 V). Legend: Charging rate @ Starting charging voltage @ Temperature @ SOH.

In this contribution, the general extraction conditions for PCM are defined as a charging at C/3, starting from the minimum cell voltage, i.e. $V_S = V_{min}$, and at 25 °C. Thereby, three factors (F_I, F_V and F_T) are proposed to relate the charge extracted in a given HI under random conditions $q(I, V_S, T)$ to the general ones, named as extraction conditions factors in Fig. 2:

a) **C-rate.** The charging C-rate affects polarization inside the cell, resulting in the difference in cell capacity as a function of C-rate. In order to overcome this issue, the factor for a given extraction current (F_I) is defined according to Eq. (2).

$$F_I = \frac{q(C/3, V_{min}, 45)}{q(I, V_{min}, 45)} \tag{2}$$

being $q(C/3, V_{min}, 45)$ the charge of a specific HI at C/3 and $q(I, V_{min}, 45)$ the one at a given current I for the same HI. This adjustment factor is obtained from RPT$_{45}$ measurements in the SL and FL cells aged within 0 and 100 % SOC. Two different charging currents are available in a given RPT$_{45}$: C/3 and C/2, as described in Section b. Moreover, the first charge of the cycling test at 0.7C is used. The assessment of these factors at a given SOH allows to define a general expression to obtain the value of F_I for a given current I. Note that the tests have similar V_S (V_{min}) and temperature (45 °C).

b) **Voltage.** Electrochemical reactions in the electrodes of a Li-ion cell take place at specific voltage levels. Thereby, if a charge starts from a voltage greater than that of a specific reaction, the total amount of Ah stored within the cell voltage limits may vary. This issue becomes a problem in real profiles, as the operating DOD depends on the load. Hence, an adjustment factor for V_S is also considered (F_V), by means of Eq. (3).

$$F_V = \frac{q(C/3, V_S, 45)}{q(C/3, V_{min}, 45)} \tag{3}$$

11

being $q(C/3, V_{min}, 45)$ the specific HI with a complete charge. $q(C/3, V_S, 45)$ is the charge extracted in the same HI but with a given V_S. In order to assess this factor, data from the SL cell aged between 50 and 75 % of SOC is used. This data set is selected because the charging starting voltage is greater than the voltage of the first peak detected from ICA in these cells ($V_S \geq$ 3.95 V) [33]. Note that extraction current (C/3) and temperature (45 °C) are similar.

c) **Temperature.** Temperature rise promotes ionic conductivity and lowers over-potentials of the electrodes. The ageing tests and the profiles are tested at 45 °C, thereby differing from the general conditions defined. A temperature factor (F_T) is thus proposed from Eq. (4).

$$F_T = \frac{q(C/3, V_{min}, 25)}{q(C/3, V_{min}, 45)} \tag{4}$$

with $q(C/3, V_{min}, 45)$ as the charge extracted in a specific HI at 45 °C and $q(C/3, V_{min}, 25)$ its equivalent with a charge at 25 °C. This factor is assessed by means of all the cycling ageing data test available, by comparing full charges at C/3 in RPT_{25} and RPT_{45}.

Lastly, the amount of charge that can be stored within a voltage limit also depends on the degradation state of the cells. This is implicitly assumed when considering data sets from the ageing tests, which cover the whole SL lifetime.

3.2. Feature selection

When selecting HI among the options available, several aspects should be taken into account. Accuracy and robustness to ageing are generally sought, but additional considerations depending on the estimation approach could also be of interest, such as extraction time in case the test has to be interrupted, or HI availability when assessing SOH online. Some of these criteria can be analysed in advance from ageing tests, as described in Fig. 2.

The accuracy of a specific HI can be, for example, quantified by means of Pearson Correlation Coefficient (PCC). Based on the covariance (COV) of two variables A and B, PCC allows to evaluate their correlation, according to Eq. (5):

$$PCC_{A,B} = \frac{COV(A, B)}{\sigma_A \sigma_B} \tag{5}$$

with σ_A as the standard deviation of A and σ_B as the standard deviation of B. PCC varies from [-1,1], with 1 meaning a perfect positive correlation and -1 a perfect negative correlation.

If assessed during lifetime, PCC allows also to determine the robustness of HI to ageing. Hence, the proposed SOH estimation method considers the computation of PCC in the calendar and cycling ageing tests, as Fig. 2 shows, so

that a first selection criteria is obtained.

On the other hand, depending on the estimation approach in real profiles different aspects should be considered. If offline estimation is targeted, normal operation of the battery is interrupted to extract HIs. The duration of this pause should be minimized in order to decrease its impact in performance, and therefore extraction time is also a parameter of interest in this case, as pictured in Fig. 2.

3.3. SOH model

Once the HI is selected, it is related to the overall capacity of the cell by means of a SOH estimation model. In the choice of the specific SOH estimation algorithm, several aspects could be discussed, such as accuracy, implementation easiness, computational complexity or data set requirements [17]. Although Li-ion battery ageing is in general a complex process, some HIs and SOH show an approximately linear relationship, which can be captured by algorithms such as linear regression (LR). This approach allows to ease modelling and mathematical procedures, and it will be used in this contribution. In order to consider possible non-linearities, Support Vector Regression with Radial Basis kernel (SVR-RBF) will also be applied.

To train and test the SOH model, a cross-validation procedure is followed, so that the robustness of the model is enhanced. When it comes to data prediction, if the RMSE from the training set was selected to assess the expected prediction error, the goodness of the model would be overestimated. Therefore, a separate validation set is drawn from the same population as the training set, without being used for parameter estimation. The model is tested in this remaining fold, quantifying its accuracy. This procedure is repeated k times, being k the number of folds equally sized in which the initial data is divided. The cross-validation error is then computed as the average of the k testing errors, and the final parameters values are also computed from the average of the k training models.

As Fig. 2 shows, the SOH estimation model is obtained from the cycling and calendar ageing tests. Then, this model is used when assessing SOH in real profiles.

The accuracy of SOH and estimation will be evaluated by means of root mean square error and maximum absolute error, computed according to Eq. (6) and (7) respectively.

$$RMSE = \sqrt{\frac{\sum_{i=1}^{n}(Y_i - \hat{Y}_i)^2}{n}} \tag{6}$$

$$MaxAE(\%) = max\left(\frac{|SOH_i - \hat{SOH_i}|}{SOH_i}\right) \cdot 100 \qquad (7)$$

being Y the measured value, $\hat{Y}$ the estimation and n the size of the sample.

4. Case studies

Two SL real profiles are assessed in this contribution: a residential household with PV generation and a fast charge station for an electric bus. In both cases, data from real operating conditions are used. This section describes the original scenarios and the energy management strategies implemented. Both case studies are simulated and adapted to cell testing levels by energy scaling, as described in Section 2.2.2.

4.1. Case study 1: residential self-consumption

This scenario focuses on a residential household with PV generation and a storage system. The energy management strategy of the system aims to maximise the self-consumption rate of the house, as well as to reduce the power contracted from the grid. The real load data is obtained from a household located near the city of Pamplona (Spain), which has a daily average energy consumption of 10 kWh and a yearly peak power of 6 kW. The PV installation provides 4.5 kWp, and real generation measurement are also considered. The energy storage system of this scenario stands 4 kWh/4 kW.

The energy management strategy of the system has three goals. First, it is desired to maximise self-consumption. To do so, PV power is used when available to respond demand. If there is a power excess, battery is charged, and energy is ultimately delivered to the grid in case the battery is already fully charged. Second, the contracted power from the grid is intended to be reduced from 6 kW to 4 kW. Battery operating SOC is thereby restricted to values over 20 %, so that there is a margin to implement the demand peak shaving strategy. Finally, bill lowering is also targeted. Spanish hourly pricing promotes night consumption, with lower billing. Hence, a night charge is programmed in order to respond to load demand at the beginning of the day using the battery. Thereby, this demand is met with grid consumption shifted to the lowest electricity price range.

Fig. 4a) shows one day of current and voltage profiles evolution measured on the SL cell tested under the residential profile at a given day as an illustrative example. The real operating conditions have been scaled to cell level, as explained in Section 2. As can be seen, the typical operation of the cell in the residential household in a day starts with the night charge (1), followed by a sequence of charges and discharges consequence of the combination between PV generation and energy demand of the household (2).
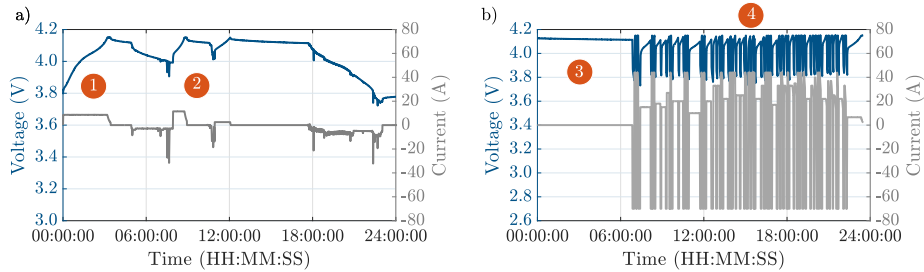
Figure 4: Cell voltage and current in a) residential profile and b) electric bus charge station profile.

4.2. Case study 2: electric bus fast charging station

In this case, a fast charging station for electric buses is analysed. The real installation is located in Pamplona (Spain), from which real operating data is obtained. The charging station receives 4 buses per hour during daytime, on working days from Monday to Saturday. The peak power demanded by the regular charge of the buses is 215 kW, and the stationary energy storage system stands 80 kWh.

The goal of this energy management strategy is to reduced the amount of demanded power from the grid by the charging station from 215 kW to 85 kW by means of a stationary storage system, in such a way that the electricity bill of the installation is reduced and the reliability of grid operation is enhanced. The overall performance of the system is as follows: when the station receives an electric bus, the vehicle is charged with the maximum allowed grid power (85 kW) and the stationary battery providing the difference required by the load. On the other hand, if there is no bus, the stationary battery of the station is charged from the grid with a power value depending on the available time. This timing depends on the next bus to come to the station, and it is known in advance from the location sent on real time by the buses. Only when it is not possible to fully charge the stationary battery of the station with the available time, maximum power is used. The fast charging station receives buses around 30 % of the operating time. During the remaining 70 % of the operating time, the stationary battery located in the station is charged from the grid. Further information of the energy management strategy and its sizing can be found in [35].

Fig. 4b) shows the operating voltage and current profiles of the SL tested with the EV charge station scenario in an illustrative day. As can be seen, there is an initial rest during the night (3), corresponding to the lack of buses in operation. Then, it can be seen how the cell responds to several partial cycles during the day, as a consequence of the bus traffic on the station (4). As the figure depicts, there are more charges per day than in the residential household, given the more dynamic character of this profile.

15

5. Results and discussion

5.1. Feature identification and analysis in ageing tests

PCM is applied to the experimental data sets of the cycling and calendar ageing tests according to the procedure described in Section 3.1.1. As explained in Section 2.2.2, several ageing conditions are considered, so that robustness of HIs can be assessed. Fig. 5 presents the different degradation trends of the cells, obtained from the 86 RPT_{25} measurements available. As can be seen in Fig. 5a) the SOH analysed ranges from 91.4 % to 24.5 %, thereby allowing to assess a very wide SL lifetime range. Moreover, Fig. 5b) shows the different ageing trends of capacity loss (ΔC), defined as the ratio between the actual capacity and its value at the beginning of the test. For example, the cell aged with a SOC range from 0 to 100 % had 42.8 % of its initial capacity after cycling 70,770 Ah, while the one between SOC of 50 and 60 % kept 91.6 %. Hence, comparing ΔC at this point, it was almost seven times greater when cycling from 0 to 100 % SOC than from 50 to 60 %. In general, higher DOD levels lead to faster degradation, and it should also be noted the differences between FL and SL samples, with increased capacity loss in these last. On the other hand, the cell aged under calendar conditions was stored during 600 days, covering a SOH range from 72.3 % to 37.4 %. In total, 18 RPT_{25} were tracked, and the degradation trend is depicted in Fig. 5c). After 600 days, the cell had kept 51.8 % of its initial capacity, as can be seen in Fig. 5d).

These ageing test results are used as input data for the SOH estimation model. PCM is applied in such a way that results are sorted based on HI and all ageing conditions mixed. In order to find an accurate and robust solution, PCC between HI and SOH is computed for the 45 HIs by means of Eq. 5. Fig. 6a) shows the results obtained, with the PCC value of the corresponding HIs. High PCC values mean greater correlation between HI and SOH and ageing robustness, and as a result HIs will be sorted in descending order as selection criteria. As could be expected, HIs with greater voltage range, such as HI 9 or HI 17, show the best results, given that the measured charge is more similar to the overall cell capacity.

As HI selection criteria for offline SOH estimation, extraction time is evaluated in the 45 HIs at three SOH levels (91 %, 57 % and 40 %), being the average results presented in Fig. 6b). As can be seen, in general the higher extraction times correspond to greater values of PCC. This could be expected, as the more charge used in the HI, the more time required and the more similar the HI is to the overall capacity of the cell. It can also be seen how the extraction time decreases as the cells age, which could be expected given the Ah counting approached used in PCM. Hence, considering as an example HI 9, the average values go from 129 minutes required at 91 % of SOH to 44 minutes with SOH of 40 %. Nevertheless, the extraction time reduction is dependent on the HI, as for example HI 45 only decreases from 20 to 10 minutes between 91 % and 40 % of SOH. Therefore, a compromise between both accuracy and extraction
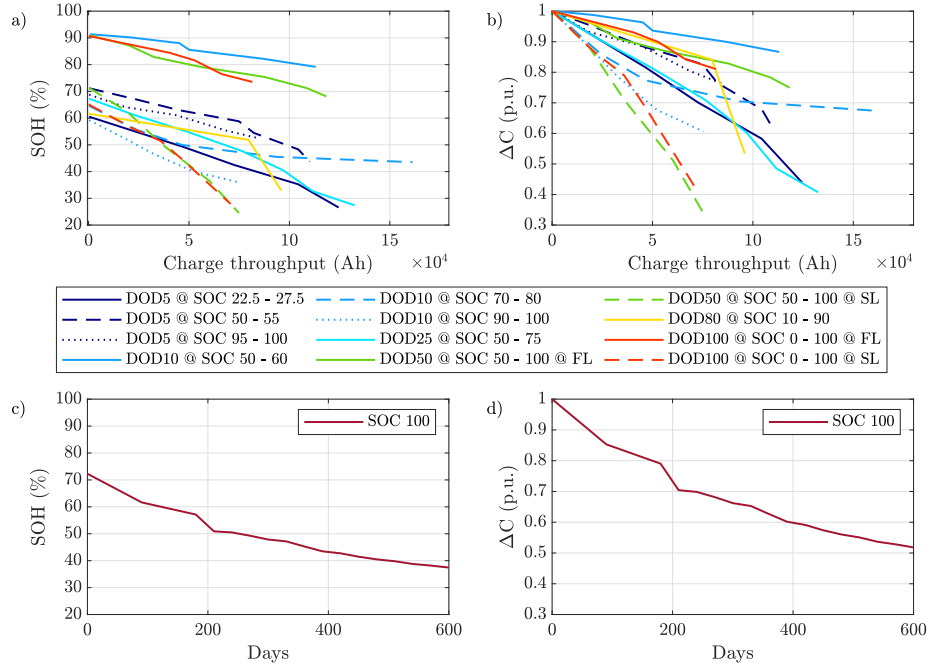
Figure 5: Experimental results of the ageing tests: cycling results in terms of a) SOH measurements with the corresponding total charge throughput, b) capacity loss with total charge throughput; calendar ageing results in terms of c) SOH measurements with the corresponding time lapse and d) capacity loss.

time should ideally be found to select HI for offline SOH estimation.

On the other hand, online estimation may require the adjustment of the extraction conditions. To this end, the adjustment factors F_I, F_V and F_T are obtained from the ageing test data, as described in Section 3.1.2. As an illustrative example, the values of these factors for HI 39 are depicted in Fig. 7. The evolution of F_I, computed at C/3, C/2 and 0.7C at different SOH is presented in Fig. 7a). As can be seen, F_I increases as the cell ages, especially at high C-rates. This is in good agreement with the impact of internal resistance rise, which leads to a faster achievement of the voltage limits of the HI and consequently of lower charge extracted in the interval. In addition, other aspects such as active material reduction and electrode failures also contribute to this factor increasing as the cell degrades. The generalisation to other C-rates is carried out by fitting a second-order polynomial between the measurements for a given SOH (SOH_i), as expressed in Eq. 8. The coefficients of the polynomial expression are then computed for the different SOH levels available, so that the influence of ageing is considered. The precise values of these coefficients can be found in the Supplementary material. When it comes to FV and FT, an upward tendency with ageing is found, as can be seen in Fig. 7b) which is consistent
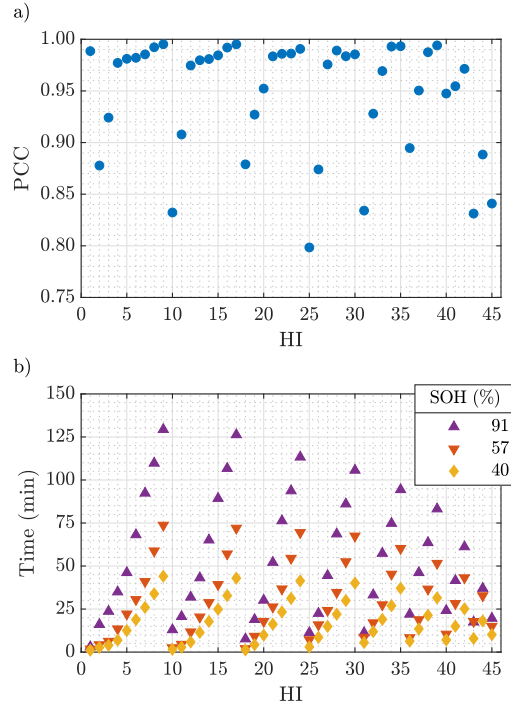
17

Figure 6: a) Pearson correlation coefficient and b) extraction time at different SOH of the 45 HIs.

with the impact of operating conditions as the cell degrades. Therefore, they will be assessed as a look-up table for each HI depending on the specific SOH, which can also be found in the Supplementary material.

$$F_I(I, SOH) = a_0(SOH) + a_1(SOH) \cdot I + a_2(SOH) \cdot I^2 \tag{8}$$

5.2. SOH estimation in real profiles

The SOH estimation method described in Section 3 is validated with the experimental testing of a FL and a SL cell under the real operating profiles explained in Section 4, i. e. the residential household with PV generation and energy storage and the fast charging station for electric buses.

5.2.1. Offline

The first estimation approach is validated considering the periodical RPT measurements in the profiles. For a given HI, the corresponding estimation model is firstly trained and tested with the cycling and calendar ageing tests, as explained in Section 3. On a second stage, the RPT_{25} measurements carried out in the the profiles allow to obtain the HIs during the test. Considering all
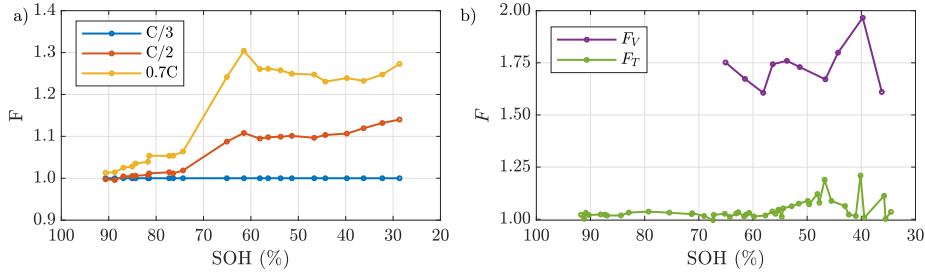
18

Figure 7: a) Current factor measured at C/3, C/2 and 0.7C and b) voltage and temperature factors as a function of SOH in HI 39.

the results obtained in a given profile, HIs are sorted based on their PCC, and used to validate the corresponding SOH estimation model.

Fig. 8a) and b) show respectively the accuracy results for SOH estimation in the residential profile and the fast charging station of the top ten HIs in terms of PCC, sorted in descending order. Both the FL and SL samples are considered on each case, resulting in 16 and 20 validation points on each profile. Considering the best algorithm result for each HI, results are slightly better in the residential profile, with RMSE values ranging from 0.6 % of HI 9 to 2.1 % of HI 34, whereas the accuracy achieved in the fast charging profile goes from 0.8 % in HI 34 to 2.6 % in HI 1. The best results in terms of MaxAE are 1.2 % in the residential profile (HI 9) and 2.3 % in the fast charging station (HI 34).

Therefore, a more general insight on the offline estimation results is given in Fig. 8c), where all the measurements obtained in both profiles are mixed in the validation. A total of 36 points are thus used. As can be seen, RMSE ranges from 0.7 % of HI 24 to 2.8 % of HI 1. Considering MaxAE, results vary from 1.6 %, obtained in HI 24 to 8.1 % of HI 1. These differences can be explained by a combination of their correlation with SOH, quantified from PCC and the specific algorithm used.

As already mentioned, additional criteria could be desired for HI in offline SOH estimation, such as extraction time. Fig. 8d) shows the average extraction time at a SOH level of 57 %, selected as illustrative example, being both profiles considered. As can be seen, values range from less than 2 minutes in HI 1 to almost 74 minutes required in HI 9. In general, the greater voltage range of the HI, the greater the extraction time required, given that Ah counting is used. When comparing to the overall capacity test times, for this SOH, a total of 464 minutes were required. The reduction of measurement times of the proposed method compared to capacity tests is therefore clear, with 99.6 % in HI 1 and 84.1 % in HI 9.

Another aspect to consider is the impact of algorithm choice in the SOH
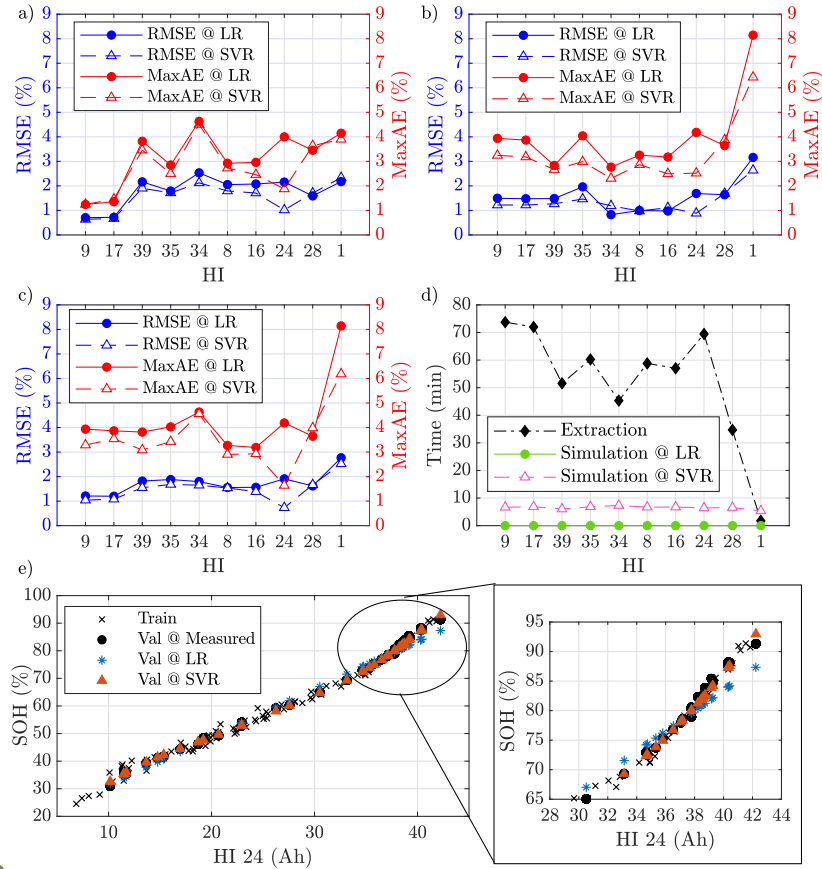
19

Figure 8: Validation results of the SOH models under fixed extraction conditions in terms of RMSE and MaxAE for a) residential profile, b) fast charging station profile and c) both profiles, d) average measurement and simulation time required at 57 % of SOH and d) example of model training and validation with all the profile data using HI 24, detailed at high SOH.

estimation model. As shown in Fig. 8c), the best accuracy results no matter of the profile tested are obtained by means of SVR-RBF with HI 24. To better illustrate this case, Fig. 8e) shows the training and validation data measured in HI 24, together with the estimation results from LR and SVR-RBF algorithms. It can be seen how the correlation between HI and SOH has a different slope in high SOH values. This change is best captured by SVR-RBF, thereby obtaining the good accuracy results reported. However, it should also be noted that computational times of SVR-RBF are greater than in the case of LR, as can be seen in Fig. 8b). For the example proposed, at 57 % of SOH, SVR-RBF requires around 6 minutes in the HI analysed for model training and testing, while LR solves the problem in few seconds.

5.2.2. Online

On the other hand, online estimation in profiles allows not to interfere in the normal operation of a battery. Given the low change rate of SOH, a weekly estimation is considered as sufficient. Hence, from the voltage measurements of the cell in a given week, charges are first selected, with their corresponding start and end voltages and charging current. An example of the operating voltage in the residential household and the electric bus charge station during a day is depicted in Fig. 4. As can be seen in the figure, the voltage profile in the fast charging station is more dynamic, and the charging starting values are generally greater.

Then, the voltage ranges are classified according to Table 3 so that the HIs available are identified. The apparition of HIs depends on the voltage profile, and therefore not all the examples gathered in the table may be available. Considering the accuracy and robustness results presented in Fig. 6a), HIs are sorted based on their PCC, and the best option is firstly targeted. Table 4 resumes the best three results on each profile using the FL and SL samples. The voltage range and PCC of the HI are also shown, together with the maximum and minimum number of identifications per week of testing. As can be seen, in case study 1 it is possible to use HIs with lower voltage ranges and resulting higher PCC than in case study 2, due to the characteristics of the operating profile. It can be seen though that the number of repetitions of a given HI is lower, as the voltage profile is less dynamic. Comparing the number of HIs identified in the FL and SL samples for a given profile, it should be noted that it is greater in the SL cell. This is a consequence of the degradation state of the cells, as the internal resistance of SL samples is greater, which result in higher voltage drops.

As explained in Section 3.1.2, it is necessary to adapt the charge measured in a given HI in terms of current, starting charge voltage and temperature, in order to avoid the influence of these factors and to compare HI under similar conditions. SOH estimation models obtained from ageing tests will be also used in this approach. In sum, considering a given Ah measurement in a HI at a certain SOH_i with current I, charging start voltage V_S and at temperature T ($q(I, V_S, 45, SOH_i)$), the input value for the SOH estimation model is obtained from Eq. 9. It should be highlighted that the extraction conditions of the models are C/3, full charge and 25 °C. The values for F_I, F_V and F_T of the specific HI are updated based on the previous SOH (SOH_{i-1}), considering the values gathered in the Supplementary material.

$$q(C/3, V_{min}, 25, SOH_i) = q(I, V_S, 45, SOH_i) \cdot F_I(SOH_{i-1}) \cdot F_V(SOH_{i-1}) \cdot F_T(SOH_{i-1})$$
(9)

Therefore, considering the available HIs in the profiles, detailed in Table 4, and after adjusting the extraction conditions, the SOH estimation models are validated in the SL operating profile. Fig. 9 shows an example of SOH estimation in the SL samples tested under the residential profile (Fig. 9a) and the fast

Table 4: HIs available on the real profiles from the experimental testing of the FL and SL cells, with their voltage ranges, PCC and maximum (Max) and minimum (Min) number of measurements per week.

Case study	Cell	HI	Voltage range (V)	PCC	Max	Min
1	FL	39	3.95 - 4.15	0.994	5	1
		35	3.90 - 4.15	0.993	4	1
		34	3.90 - 4.10	0.993	4	1
	SL	39	3.95 - 4.15	0.994	8	2
		35	3.90 - 4.15	0.993	5	1
		34	3.90 - 4.10	0.993	6	1
2	FL	41	4.00 - 4.10	0.955	12	1
		40	4.00 - 4.05	0.947	23	1
		44	4.00 - 4.15	0.888	33	17
	SL	42	4.00 - 4.15	0.997	212	3
		41	4.00 - 4.10	0.955	255	4
		40	4.00 - 4.05	0.947	262	6

charging station profile (Fig. 9b) during the tests. As can be seen in the figure, the HI used on each case as input for the models are HI 39 and HI 42 respectively, as a result of the available voltage ranges on each case. The estimation carried out through SVR is generally more accurate than using LR, as can be seen especially in Fig. 9b).

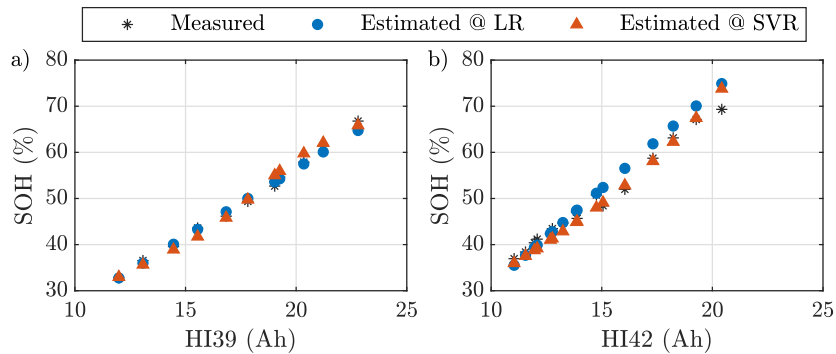Figure 9: Validation results of the SL real profiles, with SOH measured and estimated through LR and SVR in the SL cells tested under a) the residential profile and b) the fast EV charging station.

From the estimated values, the error considering the measured SOH was computed weekly, and the corresponding RMSE and MaxAE for each case study and sample were obtained. Table 5 shows the accuracy results considering LR

and SVR in the SL profiles, detailed for each cell tested. The HI used, as well as the number of weeks and the SOH range covered are also shown. The total number of weeks available on each profile varies depending on the duration of the test. Furthermore, some measurement errors were identified during the test, and as a result the corresponding HIs tracked during these weeks were considered as outliers. For its part, the HI selected depends on the availability during the test. For example, in the FL cell aged under the fast charging station profile, HI41 and HI40 showed higher PCC values, as shown in Table 4. However, some weeks they were only tracked once, and therefore HI44 was considered for estimation so that the impact of possible measurement errors was diminished.

As can be seen, SOH estimation in the residential case study is achieved with MaxAE below 3.2 % and RMSE of 1.6 % in the FL cell, while in SL it improves up to RMSE of 0.9 % and MaxAE of 2.0 %. In both cells, HI 39 was used as input data for the model. On the other hand, the estimation of SOH in the fast charge station lead to RMSE below 3.0 % in the FL cell and 1.8 % in the SL sample. MaxAE achieved were 6.6 % and 4.5 % respectively. The accuracy of this case study is determined by the HI available in the profile, as both HI 42 and HI 44 showed worse PCC than HI 39. Moreover, data used to adjust F_V, obtained from the cycling ageing tests, covered a SOH range from 67.3 % to 27.4 %, which hampers the estimation in the FL cells.

Table 5: Results from estimation in profiles under real operating conditions.

Profile	Cell	Nº weeks	SOH (%)	HI	RMSE (%)		MaxAE (%)	
					LR	SVR	LR	SVR
Residential	FL	17	91.3 - 78.0	39	1.62	1.63	3.15	3.58
	SL	11	67.7 - 31.0	39	0.90	1.24	2.04	2.33
EV charge station	FL	14	88.2 - 74.9	44	3.01	2.96	6.79	6.65
	SL	16	69.3 - 36.0	42	2.52	1.82	5.58	4.47

Comparing between estimation algorithms, it is found that in general they perform similarly in the residential case study, with slightly greater performance of LR. However, when it comes to the EV fast charge station case, SVR-RBF allows a better estimation, especially in the SL sample. As explained in the offline assessment, this algorithm captures the non-linearity of HI with SOH, and therefore it may be a good choice when a HI with lower PCC is used. To have a context with other research contributions that target online SOH estimation in SL, [24] achieved SOH online estimation with RMSE lower than 1.45 % by ageing under synthetic cycling profiles reused cells from 80 to 45 % of SOH. From its part, [10] reached errors below 1.52 % estimating SOH in a retired module aged also under synthetic procedures from 94 % to 62 % of SOH. The real profiles tested in this contribution, which differ from the model, together with the wider SOH range covered, encourages the use of this method

to other operating profiles, given the satisfactory results achieved.

6. Conclusion

This contribution focuses on the SOH estimation in real profiles. To this end, two promising scenarios for second-life batteries are analysed: residential self-consumption with PV generation and a fast charging station for an electric bus. The differences in operating conditions between both profiles allow to have a general insight on this issue.

Partial charging method is the extraction approach selected for health indicators. Robustness to ageing is assessed by means of cycling and calendar ageing tests, with a total of 11 different ageing conditions and 13 cells tested. As a result, a wide SOH range from 91.4 % to 24.5 % is covered, which allows to evaluate SL lifetime completely. These data are used as input for the SOH model, while the experimental results of two cells aged under each real profile are used for validation. As estimation algorithms, LR and SVR-RBF are considered.

SOH estimation is assessed with both offline and online approaches. First, from periodical RPT in both ageing tests and profiles, HIs are extracted under similar conditions. Validation results show that it is possible to estimate SOH in the residential profile with RMSE of 0.6 % and maximum errors of 1.2 %, while in the fast charging station the RMSE achieved is 0.8 % and the maximum error is 2.3 %. Time reduction compared to capacity test is 85 % in average considering the fastest HI. Therefore, accurate and robust HI are proposed, which allow to decrease testing times significantly.

When it comes to online SOH estimation, the operating conditions of the profiles are adapted to the RPT, by means of adjustment factors of current, voltage and temperature previously defined from the cycling ageing tests. Weekly assessment results in RMSE below 1.3 % in the residential case study and 3.6 % in the charging station. Completing the SOH range of adjustment factors is recommended, as if validation set is within it, RMSE decreases to 1.8 % in this case study.

Overall, the proposed SOH estimation method allows to assess SL real profiles under both offline and online approaches. The resulting reduction of testing times and procedures contributes to the health assessment of retired EV batteries online in their second use, thereby reinforcing the economic viability of this market. The analysis of other operating profiles and the extrapolation to other chemistries are regarded as further lines for this work.

7. Acknowledgements

References

[1] International Energy Agency, Global EV Outlook 2021, Tech. rep., International Energy Agency (2021). `doi:10.1787/d394399e-en`.

[2] E. Martinez-Laserna, I. Gandiaga, E. Sarasketa-Zabala, J. Badeda, D. I. Stroe, M. Swierczynski, A. Goikoetxea, Battery second life: Hype, hope or reality? A critical review of the state of the art, Renewable and Sustainable Energy Reviews 93 (February 2017) (2018) 701–718. `doi: 10.1016/j.rser.2018.04.035`.

[3] E. Hossain, D. Murtaugh, J. Mody, H. M. R. Faruque, M. S. Haque Sunny, N. Mohammad, A Comprehensive Review on Second-Life Batteries: Current State, Manufacturing Considerations, Applications, Impacts, Barriers & Potential Solutions, Business Strategies, and Policies, IEEE Access 7 (c) (2019) 73215–73252. `doi:10.1109/ACCESS.2019.2917859`.

[4] F. Mathieux, F. Di Persio, P. Tecchio, A. Pfrang, U. Eynard, A. Podias, M. Cusenza, S. Bobba, M. Messagie, Sustainability Assessment of Second Life Application of Automotive Batteries (SASLAB) : JRC exploratory research (2016-2017) : final technical report, August 2018, Publications Office, 2018. `doi:doi/10.2760/53624`.

[5] N. Horesh, C. Quinn, H. Wang, R. Zane, M. Ferry, S. Tong, J. C. Quinn, Driving to the future of energy storage: Techno-economic analysis of a novel method to recondition second life electric vehicle batteries, Applied Energy 295 (2021) 117007. `doi:https://doi.org/10.1016/j.apenergy. 2021.117007`.

[6] I. Mathews, B. Xu, W. He, V. Barreto, T. Buonassisi, I. M. Peters, Technoeconomic model of second-life batteries for utility-scale solar considering calendar and cycle aging, Applied Energy 269 (2020) 115127. `doi:https://doi.org/10.1016/j.apenergy.2020.115127`.

[7] T. Steckel, A. Kendall, H. Ambrose, Applying levelized cost of storage methodology to utility-scale second-life lithium-ion battery energy storage systems, Applied Energy 300 (2021) 117309. `doi:https://doi.org/10. 1016/j.apenergy.2021.117309`.

[8] Z. Song, S. Feng, L. Zhang, Z. Hu, X. Hu, R. Yao, Economy analysis of second-life battery in wind power systems considering battery degradation in dynamic processes: Real case scenarios, Applied Energy 251 (2019) 113411. `doi:https://doi.org/10.1016/j.apenergy.2019.113411`.

[9] E. Braco, I. San Martín, A. Berrueta, P. Sanchis, A. Ursúa, Experimental Assessment of First- And Second-Life Electric Vehicle Batteries: Performance, Capacity Dispersion, and Aging, IEEE Transactions on Industry Applications 57 (4) (2021) 4107–4117. `doi:10.1109/TIA.2021.3075180`.

[10] Q. Zhang, X. Li, Z. Du, Q. Liao, Aging performance characterization and state-of-health assessment of retired lithium-ion battery modules, Journal of Energy Storage 40 (May) (2021) 102743. `doi:10.1016/j.est.2021.102743`.

[11] E. Braco, I. San Martín, A. Berrueta, P. Sanchis, A. Ursúa, Experimental assessment of cycling ageing of lithium-ion second-life batteries from electric vehicles, Journal of Energy Storage 32 (July) (2020) 101695. `doi:10.1016/j.est.2020.101695`.

[12] C. White, B. Thompson, L. G. Swan, Repurposed electric vehicle battery performance in second-life electricity grid frequency regulation service, Journal of Energy Storage 28 (November 2019) (2020) 101278. `doi:10.1016/j.est.2020.101278`.

[13] S. J. Tong, A. Same, M. A. Kootstra, J. W. Par, Off-grid photovoltaic vehicle charge using second life lithium batteries: An experimental and numerical investigation, Applied Energy 104 (2013) 740–750. `doi:https://doi.org/10.1016/j.apenergy.2012.11.046`.

[14] M. Ahmeid, M. Muhammad, S. Lambert, P. S. Attidekou, Z. Milojevic, A rapid capacity evaluation of retired electric vehicle battery modules using partial discharge test, Journal of Energy Storage 50 (March) (2022) 104562. `doi:10.1016/j.est.2022.104562`.

[15] Y. Zhang, Y. Li, Y. Tao, J. Ye, A. Pan, X. Li, Q. Liao, Z. Wang, Performance assessment of retired EV battery modules for echelon use, Energy 193 (2020) 116555. `doi:10.1016/j.energy.2019.116555`.

[16] T. Waldmann, B. I. Hogg, M. Wohlfahrt-Mehrens, Li plating as unwanted side reaction in commercial Li-ion cells – A review, Journal of Power Sources 384 (November 2017) (2018) 107–124. `doi:10.1016/j.jpowsour.2018.02.063`.

[17] X. Sui, S. He, S. B. Vilsen, J. Meng, R. Teodorescu, D. I. Stroe, A review of non-probabilistic machine learning-based state of health estimation techniques for Lithium-ion battery, Applied Energy 300 (January) (2021). `doi:10.1016/j.apenergy.2021.117346`.

[18] M. Berecibar, I. Gandiaga, I. Villarreal, N. Omar, J. Van Mierlo, P. Van Den Bossche, Critical review of state of health estimation methods of Li-ion batteries for real applications, Renewable Sustainable Energy Reviews 56 (2016) 572–587. `doi:10.1016/j.rser.2015.11.042`.

[19] F. Luo, H. Huang, L. Ni, T. Li, Rapid prediction of the state of health of retired power batteries based on electrochemical impedance spectroscopy, Journal of Energy Storage 41 (May) (2021) 102866. `doi:10.1016/j.est.2021.102866`.

[20] J. Meng, L. Cai, D. I. Stroe, J. Ma, G. Luo, R. Teodorescu, An optimized ensemble learning framework for lithium-ion Battery State of Health estimation in energy storage system, Energy 206 (2020) 118140. `doi:10.1016/j.energy.2020.118140`.

[21] S. Vilsen, D. I. Stroe, Battery state-of-health modelling by multiple linear regression, Journal of Cleaner Production 290 (2021) 125700. `doi:10.1016/j.jclepro.2020.125700`.

[22] L. Cai, J. Meng, D. I. Stroe, G. Luo, R. Teodorescu, An evolutionary framework for lithium-ion battery state of health estimation, Journal of Power Sources 412 (November 2018) (2019) 615–622. `doi:10.1016/j.jpowsour.2018.12.001`.

[23] Y. Jiang, J. Jiang, C. Zhang, W. Zhang, Y. Gao, N. Li, State of health estimation of second-life LiFePO4 batteries for energy storage applications, Journal of Cleaner Production 205 (2018) 754–762. `doi:10.1016/j.jclepro.2018.09.149`.

[24] W. Xiong, Y. Mo, C. Yan, Online State-of-Health Estimation for Second-Use Lithium-Ion Batteries Based on Weighted Least Squares Support Vector Machine, IEEE Access 9 (2021) 1870–1881. `doi:10.1109/ACCESS.2020.3026552`.

[25] X. Lai, C. Deng, J. Li, Z. Zhu, X. Han, Y. Zheng, Rapid sorting and regrouping of retired lithium-ion battery modules for echelon utilization based on partial charging curves, IEEE Transactions on Vehicular Technology 70 (2) (2021) 1246–1254. `doi:10.1109/TVT.2021.3055068`.

[26] E. Schaltz, D.-I. Stroe, K. Nørregaard, B. Johnsen, A. Christensen, Partial charging method for lithium-ion battery state-of-health estimation, in: 2019 Fourteenth International Conference on Ecological Vehicles and Renewable Energies (EVER), 2019, pp. 1–5. `doi:10.1109/EVER.2019.8813645`.

[27] S. Zhang, B. Zhai, X. Guo, K. Wang, N. Peng, X. Zhang, Synchronous estimation of state of health and remaining useful lifetime for lithium-ion battery using the incremental capacity and artificial neural networks, Journal of Energy Storage 26 (2019) 100951. `doi:https://doi.org/10.1016/j.est.2019.100951`.

[28] R. Xiong, L. Li, J. Tian, Towards a smarter battery management system: A critical review on battery state of health monitoring methods, Journal of Power Sources 405 (2018) 18–29. `doi:https://doi.org/10.1016/j.jpowsour.2018.10.019`.

[29] P. Kubiak, Z. Cen, C. M. López, I. Belharouak, Calendar aging of a 250 kW/500 kWh Li-ion battery deployed for the grid storage application, Journal of Power Sources 372 (July) (2017) 16–23. `doi:10.1016/j.jpowsour.2017.10.063`.

[30] Z. Xu, J. Wang, P. D. Lund, Y. Zhang, Co-estimating the state of charge and health of lithium batteries through combining a minimalist electrochemical model and an equivalent circuit model, Energy 240 (2022) 122815. `doi:https://doi.org/10.1016/j.energy.2021.122815`.

[31] X. Feng, C. Weng, X. He, X. Han, L. Lu, D. Ren, M. Ouyang, Online state-of-health estimation for li-ion battery using partial charging segment based on support vector machine, IEEE Transactions on Vehicular Technology 68 (9) (2019) 8583–8592. `doi:10.1109/TVT.2019.2927120`.

[32] E. Braco, I. San Martin, P. Sanchis, A. Ursúa, D.-I. Stroe, Health indicator selection for state of health estimation of second-life lithium-ion batteries under extended ageing, Journal of Energy Storage 55 (2022) 105366. `doi:https://doi.org/10.1016/j.est.2022.105366`.

[33] E. Braco, I. San Martin, A. Ursúa, P. Sanchis, Incremental capacity analysis of lithium-ion second-life batteries from electric vehicles under cycling ageing, in: 2021 IEEE International Conference on Environment and Electrical Engineering and 2021 IEEE Industrial and Commercial Power Systems Europe (EEEIC / I CPS Europe), 2021, pp. 1–6. `doi:10.1109/EEEIC/ICPSEurope51590.2021.9584637`.

[34] A. Barai, K. Uddin, M. Dubarry, L. Somerville, A. McGordon, P. Jennings, I. Bloom, A comparison of methodologies for the non-invasive characterisation of commercial Li-ion cells, Progress in Energy and Combustion Science 72 (2019) 1–31. `doi:10.1016/j.pecs.2019.01.001`.

[35] I. Ojer, A. Berrueta, J. Pascual, P. Sanchis, A. Ursúa, Development of energy management strategies for the sizing of a fast charging station for electric buses, in: 2020 IEEE International Conference on Environment and Electrical Engineering and 2020 IEEE Industrial and Commercial Power Systems Europe (EEEIC / I CPS Europe), 2020, pp. 1–6. `doi:10.1109/EEEIC/ICPSEurope49358.2020.9160716`.